

Long-term evolution of transient liquid water on Mars

Mark I. Richardson

Division of Geological and Planetary Sciences, California Institute of Technology, Pasadena, California, USA

Michael A. Mischna

Jet Propulsion Laboratory, California Institute of Technology, Pasadena, California, USA

Received 28 September 2004; revised 3 December 2004; accepted 23 December 2004; published 10 March 2005.

[1] Liquid water is not currently stable on the surface of Mars; however, transient liquid water (ice melt) may occur if the surface temperature is between the melting and boiling points. Such conditions are met on Mars with current surface pressures and obliquity due to the large diurnal range of surface temperatures. This yields the potential for transient, nonequilibrium liquid water. A general circulation model is used to undertake an initial exploration of the variation of this “transient liquid water potential” (TLWP) for different obliquities and over a range of increased pressures representing progressively earlier phases of Martian geological history. At higher obliquities and slightly higher surface pressures (<50 mbar), TLWP conditions are met over a very large fraction of the planet. As the surface pressure is increased above about 50–100 mbar, however, increased atmospheric thermal blanketing reduces the diurnal surface temperature range, essentially eliminating the possibility of even transient liquid water. At high enough pressures, the mean temperature is sufficiently elevated to allow stable liquid water. Thus the potential for liquid water on Mars has not decreased monotonically over planetary history as the atmosphere was lost. Instead, a distinct minimum in TLWP (the “dead zone”) will have occurred during the extended period for which pressures were in the middle range between about 0.1 and 1 bar. This has direct and restrictive implications for chemical weathering and life. The fundamental conclusion of this study is largely insensitive to invocation of brines and to more detailed treatment of atmospheric radiative processes.

Citation: Richardson, M. I., and M. A. Mischna (2005), Long-term evolution of transient liquid water on Mars, *J. Geophys. Res.*, *110*, E03003, doi:10.1029/2004JE002367.

1. Introduction

[2] The discovery of gullies has reignited the debate over the possible existence of liquid water on the Martian surface presently or in the recent past [Malin and Edgett, 2000]. While observations of valley networks and putative paleolakes can be ascribed to an ancient, warm and wet climate [Carr, 1996], very young fluvial features, insofar as surface liquid water is required for their formation, are problematic. The reason for this is that liquid water in contact with the current Martian atmosphere is unconditionally unstable as the water vapor partial pressure is always orders of magnitude lower than the triple point pressure of water. The partial pressure of water vapor in the Martian atmosphere is controlled by the temperature of the principal surface reservoir of water, currently the northern residual polar ice cap, since the atmospheric circulation provides for rapid (on geological timescales) global mixing of water vapor [Jakosky and Farmer, 1982; Jakosky, 1985; Richardson and Wilson, 2002]. At roughly 200 K, the northern cap yields an average column vapor abundance of about 10 ppμm

or peak partial pressures of about 1 Pa. While the total surface pressure on Mars is near 610 Pa, the triple point pressure is defined in terms of the water vapor partial pressure and thus, contrary to popular perception, liquid water is always very far from being stable on Mars (in fact, it is incorrect to state that the Martian environment is close to the triple point for water; it is not).

[3] The case for recent liquid water on Mars is not as bleak as consideration of liquid water stability would indicate. For example, if the gullies or other young fluvial features were carved beneath a protective ice sheet [Christensen, 2003], capable of trapping vapor and allowing the vapor pressure to build, this problem can be avoided; however, we shall not explore the possibility of liquid water formation from such “insulated” sources as this. Our goal is to investigate the likelihood of forming liquid water from surface deposits of water ice. It is also possible to avoid the problem by relaxing the assumption that the liquid water is in equilibrium with the atmosphere [Ingersoll, 1970; Kahn, 1985; Hecht, 2002]. This relaxation opens up the possibility of liquid water being an active, if ephemeral, agent on the Martian surface for a very extended fraction of geological history. Such nonequilibrium or transient liquid water would be of great geochemical and biological interest.

[4] As discussed by *Ingersoll* [1970], *Kahn* [1985], and *Hecht* [2002], transient liquid water can develop during the conversion of ice to vapor if there is sufficient solar radiative heating to keep temperatures above the melting point in the face of heat losses due to sensible, latent, and thermal infrared radiative cooling. For pure water, if the total pressure of atmospheric gas exceeds 610 Pa, liquid water maybe stable against boiling (if the temperature is below the boiling point), but may still be unstable with respect to evaporation. Boiling is only of major importance as a process because it leads to a much more rapid conversion of liquid to vapor than evaporation. When the saturation vapor pressure of the liquid exceeds the total atmospheric pressure, bubble development in the interior of the liquid is allowed and dynamically favored. Bubble formation enables the vaporization of the liquid to occur throughout the full volume of liquid, rather than simply at the surface, as in the case of evaporation. Also important in an energy-limited environment like Mars, the rough and dynamic surface generated by boiling yields much more effective sensible heat transfer. Boiling thus corresponds to very much more rapid liquid-to-vapor conversion than evaporation (and thus also much faster latent cooling). This obviously only applies should a film of fluid develop on the ice during conversion to vapor. However, the very much lower latent heat of melting versus evaporation suggests that unless a very effective removal process like boiling is active, a liquid water transitory state is likely. From these arguments, a necessary-but-not-sufficient diagnostic of the transient liquid water potential (TLWP) is that surface pressures and temperatures fall between the melting point of ice and the boiling point of liquid water. These values change somewhat depending on the purity of the water. Since the study described in this paper is largely qualitative in nature, attempting to extract some understanding of the temporal and geographical changes in TLWP as various paleoclimatic parameters are varied, we choose to assume pure water. Consideration of strong brines, for example, will affect the mapping of a particular stability distribution to a given set of parameters, but will not change the fundamental story outlined in this paper, as will be demonstrated.

[5] Transient liquid water will obviously only form where there is a water source. By definition, the regions on Mars where the TLWP is highest are those that have the highest midday temperatures and are therefore least likely to retain water ice. The seasonal cycle helps in this respect by redistributing ice during the formation of the seasonal ice deposits. However, the mean surface density of ice is sufficiently low that these deposits are likely to have fully sublimated during the spring before the times of maximum insolation and surface temperatures. It is possible to design scenarios in which the small-scale topography allows water to remain trapped and concentrated on the surface [*Svitek and Murray*, 1990] well into the summer season and until the period of maximum insolation, when it becomes exposed [*Hecht*, 2002]. Here, we do not model the distribution of water, nor do we consider small-scale topographic features. In the former case, we comment on likely water availability, but more detailed calculation of water distribution is beyond the scope of this paper. In the latter case, we are more interested in the broad geographical and temporal variations in the TLWP. Small-scale topography will have

an important role in the details of where and when particular TLW deposits develop. However, in this paper we are interested in the relative ease with which liquid water could form as orbital parameters and surface pressure evolve. Small-scale topography will change the local details, but will not affect the global scale results and trends presented here.

[6] We examine scenarios corresponding to the middle and recent climate states of Mars using a general circulation model (GCM) to find locations where conditions are acceptable for liquid water. We follow the approach taken by *Haberle et al.* [2001] (henceforth H01), who used a GCM to examine this geographical distribution for current orbital parameters and surface pressures. In section 2 we provide a brief description of the GCM used in this study and the criteria for TLWP used. In section 3, we compare the GFDL Mars GCM predictions for current conditions with those published by H01, and examine the potency of the greenhouse effect generated by the GCM for higher pressures in comparison with the *Kasting* [1991] one-dimensional model. Section 4 provides the results from our modeling work, separated into studies of orbital and spin-axis change (“orbital set”) and trends in mean surface pressure (“pressure set”). We provide a summary and conclusions in section 5.

2. Model Description

[7] This study employs the Geophysical Fluid Dynamics Laboratory (GFDL) Mars GCM [*Wilson and Hamilton*, 1996; *Wilson and Richardson*, 2000; *Fenton and Richardson*, 2001; *Richardson and Wilson*, 2002; *Mischna et al.*, 2003]. As in the latter three papers, the orbital parameters forcing the pattern of solar heating (obliquity, eccentricity and argument of perihelion) are varied. In addition, the mean surface pressure is varied in specific simulations in this study (see Table 1 for parameters used). While the model includes a treatment of the water cycle [*Richardson and Wilson*, 2002], we do not examine the predicted water cycle in this paper largely because of the additional complexity added and because the primary focus and conclusion of this study do not require it. The model does include an active seasonal CO₂ cycle, involving seasonal cap formation and the cycling of surface pressure. Radiative heating within the atmosphere by dust and CO₂ gas are treated using a band model approach [*Briegleb*, 1992; *Haberle et al.*, 1982; *Hourdin*, 1992; *Burk*, 1976]. The CO₂ thermal infrared scheme of *Hourdin* [1992] is highly accurate to about 10⁴ Pa but decreasingly so at progressively higher pressures. We use this scheme up to 10⁵ Pa, but do so in order to undertake an essentially qualitative exploration of the impact of very high pressures on TLWP, and do not place quantitative emphasis on the relationship between the specific mean surface pressure and the specific resulting greenhouse warming. Further, we do not treat radiative effects of water vapor, which may become important at higher pressures, and which would again tend to increase surface temperatures via the greenhouse effect. Partially counterbalancing this, we also do not treat the radiative effects of clouds, which would tend to increase the reflectivity of the planet. We discuss the impact of these model radiative simplifications when describing the results, but note that the nature of the physical

Table 1. A Summary of the Primary Model Parameters Used for the GCM Simulations Described in This Paper

Simulation	Atmospheric CO ₂	Obliquity	Eccentricity	L_s of Perihelion
p1x_std (o25)	6 mbar	25°	0.093	251°
p2x_std	14 mbar	25°	0.093	251°
p4x_std	22 mbar	25°	0.093	251°
p8x_std	60 mbar	25°	0.093	251°
p16x_std	120 mbar	25°	0.093	251°
p32x_std	280 mbar	25°	0.093	251°
p64x_std	450 mbar	25°	0.093	251°
p128x_std	1200 mbar (1.2 bar)	25°	0.093	251°
p1x_o45 (o45)	6 mbar	45°	0.093	251°
p4x_o45	22 mbar	45°	0.093	251°
p8x_o45	60 mbar	45°	0.093	251°
p16x_o45	120 mbar	45°	0.093	251°
p64x_o45	450 mbar	45°	0.093	251°
o15	6 mbar	15°	0.093	251°
o25_pe	6 mbar	25°	0.093	71°
o25_ne	6 mbar	25°	0.	—
o35	6 mbar	35°	0.093	251°
o45_pe	6 mbar	45°	0.093	71°
o45_ne	6 mbar	45°	0.	—
o45_he	6 mbar	45°	0.13	251°
o60	6 mbar	60°	0.093	251°
o75	6 mbar	75°	0.093	251°

effect that is the major new result of this study will be unaffected by deficiencies in the treatment of radiative transfer for very specific reasons.

[8] The model is run with a resolution of 5° in latitude and 6° in longitude, with 20 vertical levels between the surface and roughly 90 km. The model includes treatment of dust aerosols, using an injection scheme that links the mass mixing ratio injected to surface-air temperature contrast. Dust is advected by the mean wind and allowed to fall at terminal velocity. The instantaneous dust distribution is used to drive an atmospheric radiative heating scheme [Briegleb, 1992; Haberle *et al.*, 1982]. The scheme provides a good fit to air temperatures for current orbital parameters and pressures [Wilson and Richardson, 2000; Richardson and Wilson, 2002]. As the surface pressure increases, the surface-air temperature contrast decreases (as will be shown) such that radiative effects due to dust become less important as the pressure increases.

3. Model Validation and Efficacy of the Model Greenhouse Warming

3.1. Surface Temperatures for the Current Climate

[9] Several papers deal with the comparison of the GFDL Mars GCM with observations [Wilson and Hamilton, 1996; Wilson, 1997; Wilson and Richardson, 2000; Fenton and Richardson, 2001; Richardson and Wilson, 2002; Wilson *et al.*, 2002; Hinson and Wilson, 2002, 2004]. For our purposes the prediction of surface temperatures and pressures (and primarily the surface temperatures for reasons to be described) are of greatest importance. For the purposes of comparison and consistency, we demonstrate the model prediction of surface temperatures using the same $L_s = 141^\circ$ Mars Global Surveyor (MGS) Thermal Emission Spectrometer (TES) data as used by H01. The GFDL model output, values taken from the H01 study (the NASA Ames Model), and TES data are shown in Figure 1. The GFDL model agrees very well with the Ames model, both models

slightly overestimating temperatures in the tropics and placing the seasonal cap edge slightly too far equatorward. Grid resolution likely explains the cap-edge discrepancy, while the radiative influence of water ice clouds on ground temperatures may be a significant, but model-neglected aspect of the surface thermal balance in the tropics. However, the models are both within the scatter of the data and are in good mutual agreement. The model seasonal pressure cycle has already been shown by Mischna *et al.* [2003]. The

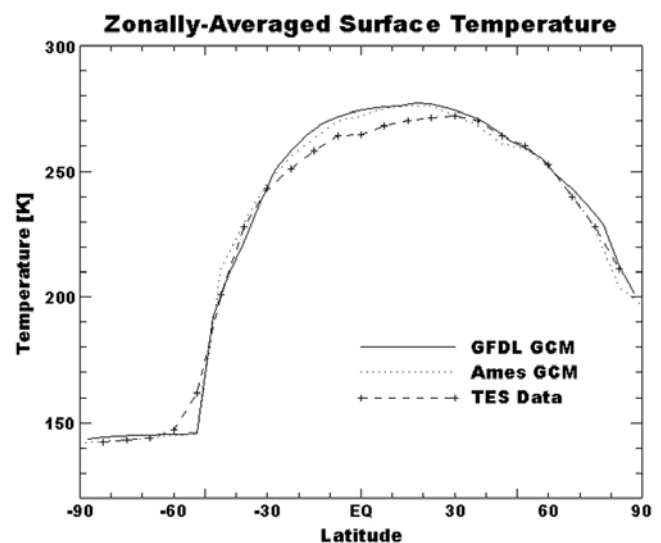


Figure 1. The distribution of zonal-mean surface temperature as a function of latitude for $L_s = 141^\circ$. Thermal Emission Spectrometer data are shown alongside output from the NASA Ames GCM (as published by H01) and the GFDL Mars GCM used in this study. The models are in very good agreement and in reasonable agreement with the data.

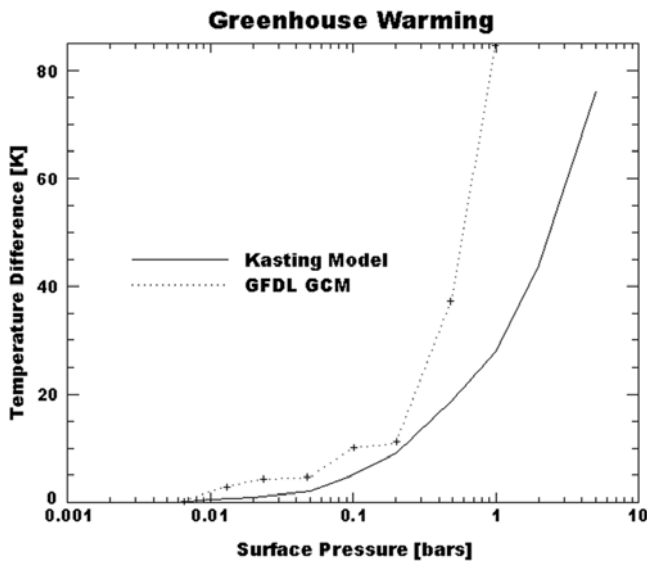


Figure 2. The increase in global-mean surface temperature with increasing global-mean surface pressure for GFDL Mars GCM used in this study and for the *Kasting* [1991] 1-D radiative-convective model. The implementation of the GCM radiation code used here has an overeffective greenhouse response, which is conservative for the purposes of this study.

cycle is in good agreement with the Viking Lander data and with the Ames GCM.

3.2. Efficacy of the Greenhouse Warming Model

[10] A significant concern for this study is the efficacy of the model greenhouse effect. This concern arises due to the known valid range of the *Houadin* [1992] thermal infrared CO₂ scheme, the model's neglect of Rayleigh scattering due to CO₂, and (perhaps most importantly) the fact that water vapor and cloud ice radiative effects are ignored. No published GCM study to date includes the effects necessary to accurately simulate the radiative environment of a higher-pressure Martian climate. In this light, it is important to understand how the net greenhouse effect generated by the model differs from that produced by a one-dimensional model that does include the appropriate radiative effects. To address these concerns, we have compared the increase in mean global surface temperature as a function of increased pressure from individual simulations in our GCM to 1-D global mean surface temperatures from *Kasting* [1991] for pressures up to ~1 bar (Figure 2).

[11] The rate of surface temperature increase with pressure is always steeper in the GCM than in the 1-D model. This begins very slowly at low pressures, but yields quite a large excess greenhouse as surface pressure increases above ~0.2 bar. Indeed, for pressures just over 1 bar, the GCM produces global mean surface temperatures that are over the melting point of water everywhere. This is at odds with the *Kasting* [1991] model and other more radiatively complete but dynamically simplified models. We assume that the one-dimensional models provide the more accurate simulation of high-pressure Martian paleoatmospheres than the GCM since there is ample reason to believe the simplified radiative treatment in this version of the GFDL Mars GCM

overpredicts the greenhouse effect (it should be noted that this is not a general statement about the GFDL Mars GCM but is specific to the particular implementation of the radiation scheme we use in this study). Specifically, the CO₂ radiative transfer scheme is known to have error growth above about 0.1 bar, while the inclusion of atmospheric emissivity due to dust also tends to increase the greenhouse effect. Thankfully, for the purposes of this study, an overactive greenhouse effect is a conservative factor; improvements in the radiation scheme will thus serve only to extend and strengthen the findings of this study, as will be described in sections 4 and 5.

3.3. TLWP for the Current Climate

[12] The criteria for transient liquid water potential (TLWP) are defined as temperatures between the melting point and boiling point of water. "Potential" refers to the fact that transient liquid water will only form if ice is present when the TLWP criteria are met; just because the TLWP criteria are met does not mean that transient liquid water will necessarily exist. We hence do not worry about the actual presence of water itself when mapping the TLWP.

[13] The melting point temperature is independent of pressure, while the boiling point temperature varies strongly with total pressure. Implicit in the definition of TLWP is the assumption that the generation of transient liquid water is an extremely nonequilibrium process. As such, we are not concerned with the water vapor partial pressure, which is the only important parameter for determining the equilibrium stability of water (be it ice or liquid). While the melting point temperature is fixed, the boiling point temperature depends on the total atmospheric pressure. This is the overpressure that prevents bubble formation within the fluid if the atmospheric pressure is higher than the saturation vapor pressure. Since the saturation vapor pressure is a strong function of the liquid temperature, the boiling point temperature (the temperature at which the saturation vapor pressure of liquid equals the total atmospheric pressure) is a strong function of the total atmospheric pressure as well. If the total atmospheric pressure is equal to the saturation vapor pressure of the liquid right at the melting point temperature (~6.1 mbar), then the melting and boiling point temperatures are the same. For the Earth at sea level, the boiling point temperature corresponds to a water vapor partial pressure of ~1 bar, yielding a temperature range between melting and boiling of ~100 K. At a more Mars-like pressure of 10 mbar, the range between melting and boiling is roughly 7 K.

[14] The TLWP criteria used in the examination of GCM output are then surface temperatures above the melting point of 273 K and below the boiling point, which is calculated by determining the liquid water temperature corresponding to a saturation vapor pressure having the same value as the local surface pressure. These criteria are the same as those used by H01 to examine the distribution of TLWP for the current climate. Figure 3a shows the total, cumulative number of hours per Martian year for which the criteria are met. This map is directly comparable to Figure 5 of H01. The durations shown are essentially identical. For example, the peak value in the Argyre basin shown by H01 is over 4 Martian days, while our Figure 3a shows a peak contour of 150 hours, or 6.25 days. In Hellas, a H01 peak

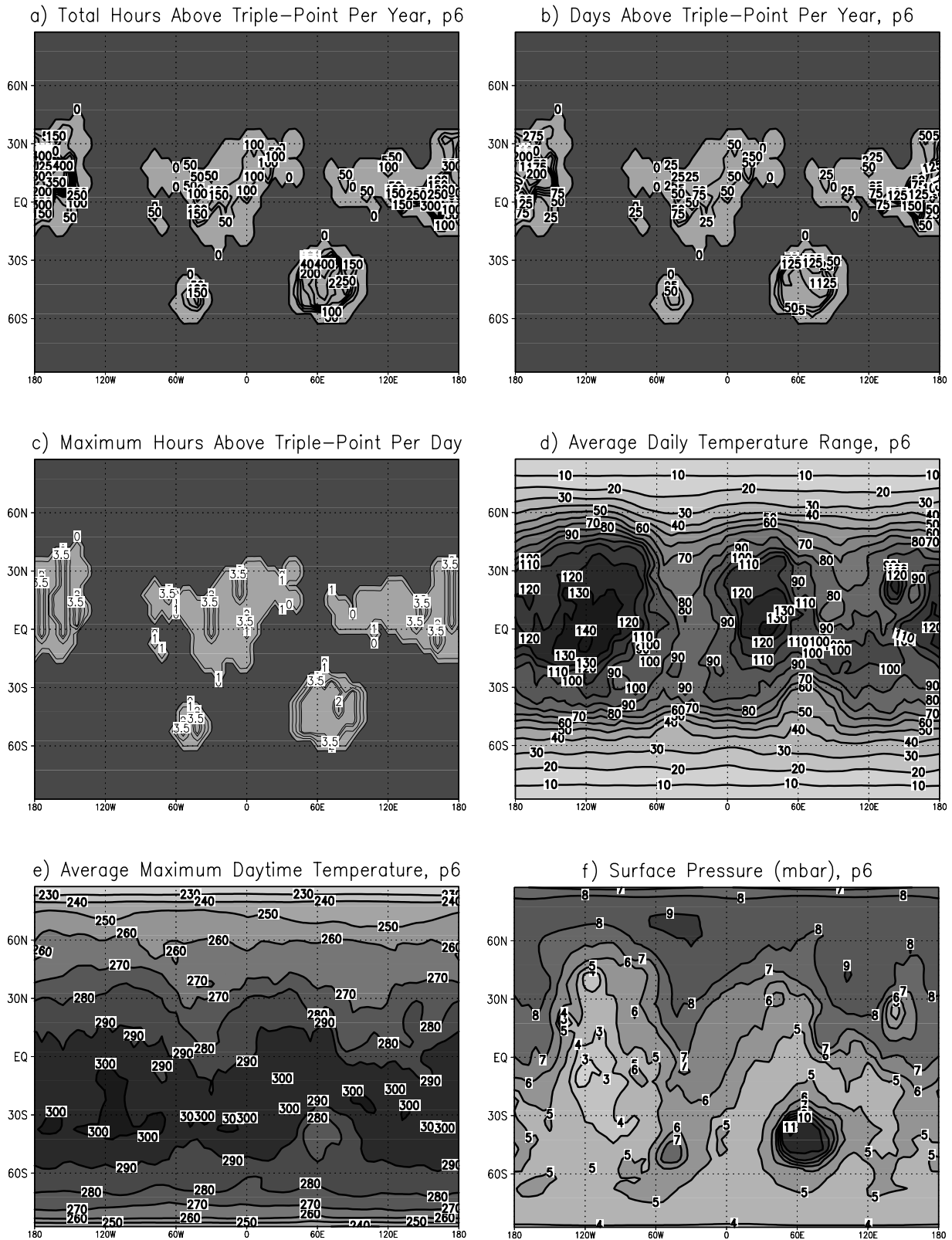


Figure 3. Predictions of TLWP for the current Martian climate, and associated climatic variables. (a) The cumulative number of hours per Martian year of TLWP. (b) The number of Martian days during which TLWP conditions were obtained. (c) The average number of hours per day when TLWP conditions were obtained. (d) The average diurnal range of surface temperatures. (e) The annual average daytime maximum surface temperatures. (f) The annual mean surface pressure.

contour of 16 days is in good agreement with our 400 hours ($16^{2/3}$ days). The spatial distributions are also very similar, with the regions satisfying the criteria located in the tropics, low thermal inertia regions, and in the Hellas and Argyre basins of the southern midlatitudes.

[15] Figure 3b shows the number of Martian days during the year for which the TLWP criteria were met for some fraction of the day. Comparison Figures 3a and 3b shows that the criteria are only met for an hour or so during each day (Figure 3c). For example, in Terra Meridiani, the hours-per-year value of about 100 and the days-per-year value of about 60 yield an average of about $1^{2/3}$ hours-per-day for those days where the TLWP criteria are reached. The hours-per-day maxima do not exceed 4 hours. Thus the TLWP criteria are only being met during the very limited portion of the diurnal cycle when surface temperatures are near their peak.

[16] The annual average temperature range is shown in Figure 3d, while the annual average daytime maximum temperature is shown in Figure 3e. The annual average daily maximum temperature exceeds 273 K over a wide swath of the planet, while the very large temperature ranges demonstrate that the mean temperatures will be very much lower than the melting point. Peak temperatures occur preferentially in the southern tropics due to the timing of perihelion just before summer solstice. The subtle influence of topography can be seen, with the deeper Hellas basin experiencing lower-than-average peak temperatures and diurnal ranges due to the added thermal inertia associated with a higher surface pressure. The high Tharsis plateau shows the opposite trend, with a maximum surface temperature range nearly three times that in the Hellas basin.

[17] The surface temperature patterns alone do not explain the TLWP distributions, as can easily be confirmed by comparing Figures 3a and 3b with Figure 3e. The surface pressure must also be considered (Figure 3f). In fact, the limitation on the TLWP distribution for the current climate results from interplay between thermal and pressure constraints. Surface temperatures establish the northernmost constraint on TLWP. At high northern latitudes it simply does not get warm enough during northern summer to permit melting. Conversely, across most of the southern hemisphere the constraint is provided by a surface pressure insufficient to have a boiling point temperature that is above the melting point temperature. Simply, surface pressures are below the triple point. This is due to the elevated topography of the southern highlands. Within the tropics, the roughly wave 2 pattern of TLWP correlates roughly with the patterns of peak daytime maximum temperature, and highlighted better in the diurnal temperature range. These are regions of low thermal inertia: the dust continents [Christensen, 1986]. However, the locations of edges of the TLWP regions do not coincide with the edges of these low-inertia regions. For example, the TLWP region including the prime meridian is much more extended than the low-inertia region between 0° and 60°E . In fact, the TLWP region extends across the high-inertia region of Chryse. Conversely, much of the low-inertia Tharsis plateau is not a region of TLWP. These deviations of TLWP from low-inertia regions are associated with topography. The elevated Tharsis plateau never experiences surface pressures sufficient to prevent boiling. The Chryse region is relatively cool

compared to other regions of the tropics, with a relatively small diurnal range of temperatures, but its low elevation yields annual-mean pressures that are up to 2 mbar above the triple point pressure. In the southern mid and high latitudes, maximum daytime temperatures are well above 273 K as far poleward as about 80°S . However, the southern highland's average surface pressure is about 1 mbar below the triple point pressure. Exceptions are noted in the deep Hellas and Argyre basins, where the largest melting-to-boiling point temperature range of anywhere on the planet is found. The regions shown in Figures 3a and 3b with the longest periods of TLWP are those that maximize both the pressure and the surface temperature maxima. However, even across Amazonis and the depths of the Hellas basin, the most favorable locations for TLWP in the present climate, the cumulative duration of TLWP never reaches 500 hours (~ 20 sols) per Martian year.

[18] Since there is no surface water ice present at any of the tropical locations shown in Figures 3a–3c with high TLWP, transient liquid water at present is also highly unlikely. While there is no permanent surface water in the southern parts of Hellas and Argyre, these regions are sufficiently poleward that water ice does accumulate in these locations as part of the seasonal ice cap in southern autumn and winter. This water ice is eventually exposed in southern spring as the seasonal CO_2 ice cap sublimates. Whether transient liquid water can form during these seasonal windows depends upon insolation and the local geometry of the surface [Hecht, 2002; Hecht and Bridges, 2003].

4. GCM Simulations of Past Climate States

[19] The numerical experiments described in this study were designed to examine the global variation of TLWP as the planetary orbital parameters (obliquity, eccentricity, and argument of perihelion) and the mean surface pressure are varied. The values for our chosen simulations are summarized in Table 1. We have chosen to examine four different but overlapping sequences of parameter variations guided by orbital models [e.g., Laskar *et al.*, 2004] and climate evolution models geared toward explaining ancient fluvial features on the Martian surface [e.g., Kasting, 1991].

[20] Holding the obliquity and exchangeable CO_2 inventory fixed, we examine the impact of eccentricity. A similar group of simulations, with the addition of a high-eccentricity case, were examined for an obliquity of 45° , which is near the long-term most-probable obliquity of Mars [Laskar *et al.*, 2004]. Simulations at current pressure and eccentricity but for obliquities spanning 15° to 75° were examined to determine the role of obliquity. An obliquity of 75° is near the maximum obtainable [Laskar *et al.*, 2004], while below 15° obliquity, the surface pressure becomes sufficiently low that no separation exists between melting and boiling. (The entire planet resides below the triple point.)

[21] The final sequence of simulations examines the impact of surface pressure. As described in section 3.3, the current mean surface pressure is marginal for TLWP and lower pressures would prohibit it for reasons mentioned above. This allows the lower value of the pressure range study to be effectively defined. The upper value is one consistent with truly stable liquid water. As shown in

section 3.2, this occurs for our model at mean pressures somewhat over 1 bar. While this is likely an underestimate of the required pressure for the reasons described, it eliminates the need to examine higher pressures for TLWP. In actuality, this pressure was found by doubling the reference pressure for each GCM simulation until stable liquid water was found. It should be noted that we do not vary the intensity of solar radiation. Although there is strong evidence that the solar luminosity was roughly 30% lower at the end of heavy bombardment than it is today [Gough, 1981], we do not have good quantitative mapping of particular mean surface pressure states to particular geological dates and hence to solar luminosity. Given this uncertainty, and the very substantial error in the mapping of the model greenhouse effect to a given mean surface pressure, we do not attempt to recreate particular climatological epochs and hence believe it clearer to hold luminosity constant in these calculations.

4.1. Orbital Parameter Variations

4.1.1. Eccentricity and Precession Variations at 25° Obliquity

[22] The distribution of TLWP is controlled by topography, determining whether a given location can have separate melting and boiling point temperatures, and by the peak daily surface temperatures, determining whether the melting point is ever reached. As discussed in section 3.3, pressure is the primary restriction in the southern hemisphere, which is dominated by the elevated highlands, while in the northern hemisphere, the primary limitation is surface temperature. Figure 4b shows that the temperature maxima are biased to the southern hemisphere. This is due to the large eccentricity of the planet (receiving nearly 45% more insolation at perihelion than at aphelion), and the current timing of perihelion during southern summer (at $L_s = 251^\circ$). Since these effects compete currently, they should be compounded if the argument of perihelion is precessed by 180° (to $L_s = 71^\circ$).

[23] An orbital state with argument of perihelion at $L_s = 71^\circ$ would have been obtained as recently as 25,000 years ago, and many tens of times over the past million years [Laskar *et al.*, 2004], so it is highly relevant. While the typical number of cumulative hours, partial days, and hours per day during which the transient liquid water criteria (Figures 4i and 4j) met for such a simulation (o25_pe) are very similar to those for current argument of perihelion, the spatial distribution is noticeably different. Strong similarities exist in the tropics, but the southern hemisphere TLWP regions in Hellas and Argyre are gone, instead replaced by a large fraction of the northern mid and high latitudes between 15°N and 75°N that has now become “activated”. For this argument of perihelion, peak daytime ground temperature maxima are biased to the northern hemisphere, with temperatures in the northern mid and high latitudes regularly reaching the melting point (Figure 4g), while the mean ranges are nearly identical (Figure 4h). Conversely, in the southern hemisphere even locations with pressures above the triple point (Hellas and Argyre), no longer have peak temperatures high enough to melt water.

[24] The high northern latitude regions satisfy the TLWP criteria in a broad area over which the seasonal ice cap extends. As such, if the water ice can be protected until the

time of maximum isolation [Hecht, 2002], it may be available for seasonal melting. As a result, signatures of chemical modification of rocks and regolith associated with recent transient liquid water are thus most likely to be found at high ($>60^\circ\text{N}$) northern latitudes. Since the region in which the criteria are met extends uniformly to $\sim 70^\circ\text{N}$ – 75°N , there is substantial overlap with the region of high subsurface hydrogen (presumably water ice) observed by the Mars Odyssey orbiter [Boynton *et al.*, 2002; Feldman *et al.*, 2002; Mitrofanov *et al.*, 2002]. It is on these high-latitude, water-rich deposits that the Phoenix Lander is scheduled to settle in 2008. While this correlation sparks initial excitement by suggesting water ice is present where TLWP criteria were regularly met as little as 25,000 years ago, it should be noted that the hydrogen deposits are located tens of centimeters beneath the surface, beneath the reach of the diurnal thermal wave, and hence almost certainly tens of degrees colder than the surface temperature.

[25] The elimination of eccentricity places Mars in a circular orbit at the mean orbital distance (simulation o25_ne). This has the effect of minimizing the maximum daytime peak temperatures (by about 10 K; compare Figures 4b, 4g, and 4i), while again barely affecting the annual average diurnal temperature ranges (Figures 4c, 4h, and 4m). The TLWP distribution for this state is intermediate between the two previous states, with the northernmost limit pushed southward by about 15° from the o25_pe simulation. The southern limit is controlled by surface pressure, and so remains unchanged; however, the northern rims of the Hellas and Argyre basins show TLWP.

4.1.2. Eccentricity and Precession Variations at 45° Obliquity

[26] As stated previously, the long-term, most likely obliquity for Mars is estimated to be near 45° [Laskar *et al.*, 2004]. As such, we undertook a set of eccentricity and precession simulations for this obliquity (Figure 5). Simulation o45 shows that the spatial pattern of TLWP is similar to the o25 case in the tropics (the tropics are correctly defined in terms of the maximum latitudinal position of the subsolar point during the year; for our purposes, we use “tropics” as a shorthand to define the region roughly between 30°S and 30°N regardless of the obliquity) and southern hemisphere, but with the midlatitude and high-latitude regions of the northern hemisphere additionally meeting the criteria (compare Figures 5d and 5e with Figures 4d and 4e). This activation of the northern high latitudes is associated with the much-increased annual average daily temperatures (Figures 5b and 4b) due to the much more poleward location of the summer solstice subsolar point. The mean surface pressure actually falls relative to the o25 case. While the available CO_2 in this simulation is no different from that of the contemporary climate simulation (o25), the larger seasonal ice caps at high obliquity, yield a lower mean surface pressure (compare Figures 5a and 4a). During the year, the range of surface pressure has a much greater amplitude than at 25° obliquity, with the minimum occurring in later northern summer [see Mischna *et al.*, 2003, Figure 1]. This reduces the duration of TLWP in the tropics as peak temperatures occur near equinox. The smaller fraction of the year during which the subsolar point falls in the “tropics” also reduces the

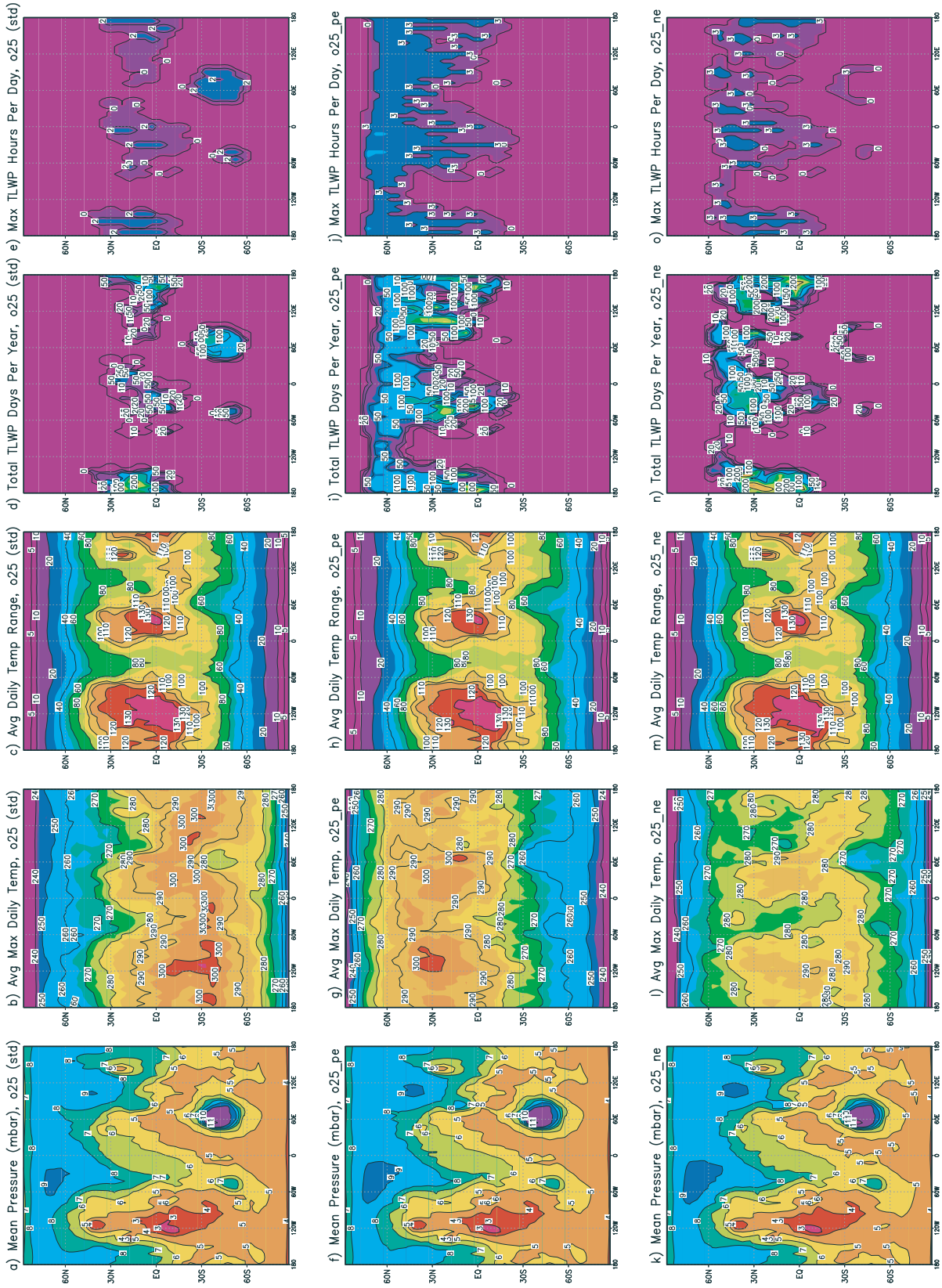


Figure 4. The annual mean surface pressure, average maximum daily surface temperatures and ranges, and the total days and maximum hours per day of TLWP for (a–e) current orbital properties, (f–j) opposite argument of perihelion, and (k–o) no eccentricity. Obliquity is 25° for each case.

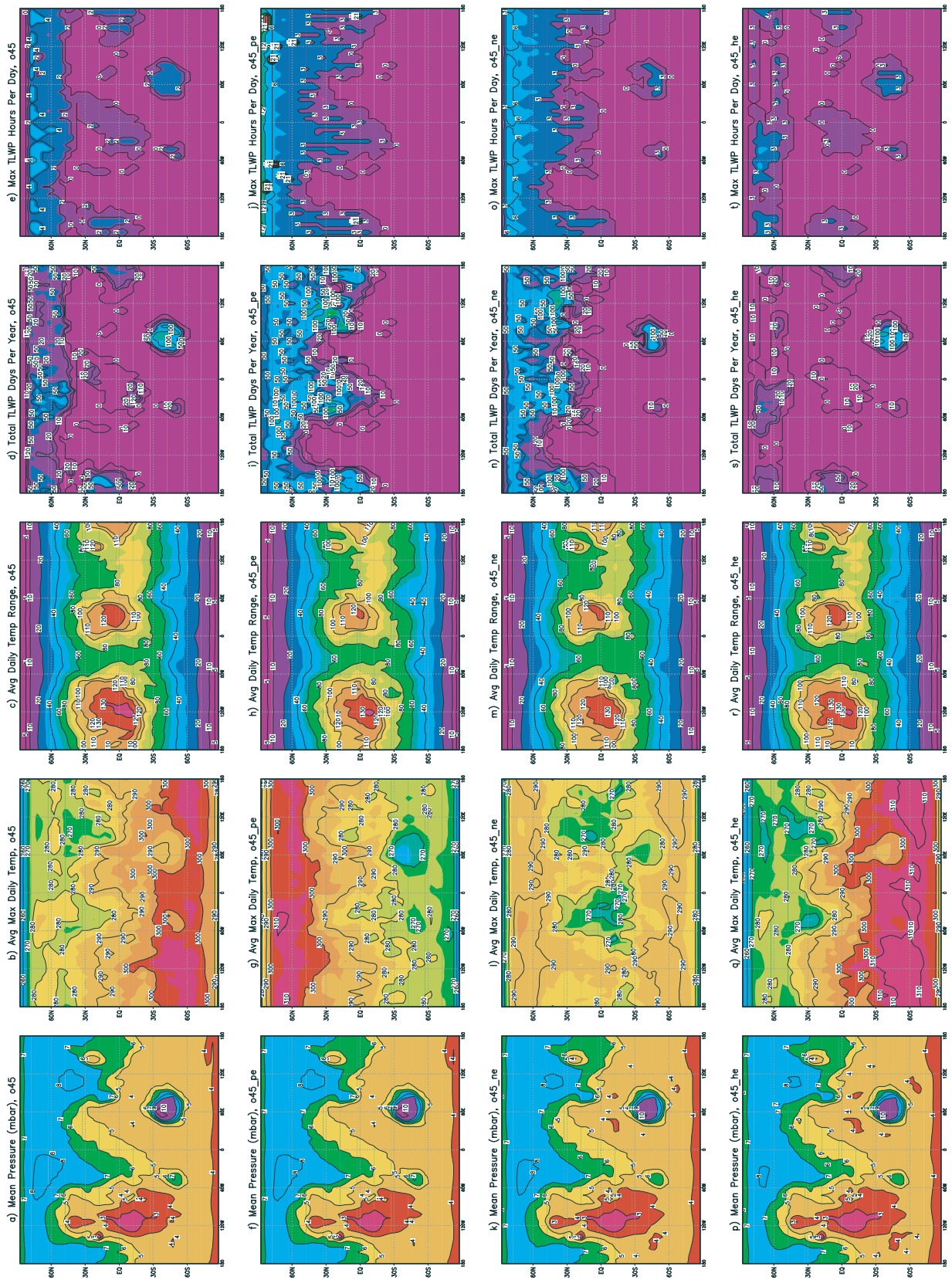


Figure 5. Same as Figure 4, but for 45° obliquity and including a simulation of high eccentricity (0.13).

TLWP duration. The distribution of TLWP extends right up to the northern residual water ice cap in the northern hemisphere in this simulation. In reality, the northern ice cap likely sublimates sufficiently to develop a deep, protective dust lag at high obliquity [Mischna *et al.*, 2003] such that it is not in contact with these very high temperatures. A substantial seasonal ice cap still forms, and the arguments made in section 4.1.1 still apply. It should also be noted that simulations including a water cycle show development of perennial tropical water ice deposits at this obliquity [Mischna *et al.*, 2003]. These deposits will have the effect of increasing albedo and thermal inertia, but are not included in this simulation, such that the nonzero TLWP shown in the tropics for 45° may not actually be obtained.

4.1.3. Obliquity Variations From 15° to 75°

[27] The effect of obliquity change from 25° to 45° has already been described in section 4.1.2. In this section, we discuss a more complete span of putative obliquities, from 15° to 75°. For 15° obliquity, the GCM predicts the formation of a permanent CO₂ ice cap and the surface pressure begins drifting to a lower equilibrium value. For this study, we take the first year of the output and do not allow the model to achieve its true mean surface pressure. The reason for this is that at pressures much below current, the entire planet would never achieve local surface pressures above 610 Pa and the trivial result of zero TLWP everywhere is obtained.

[28] The effect of obliquity on mean surface pressure can be gauged by comparison of Figures 6a (15°), 4a (25°), 6f (35°), 5a (45°), 6k (60°), and 6p (75°). As the obliquity increases, the annual mean surface pressure falls, for the reasons mentioned in section 4.1.2. In these simulations, we have assumed that the total abundance of CO₂ in the cap-atmosphere system is fixed regardless of obliquity. Maximum pressures remain nearly constant while the minimum pressures fall. The change in mean pressure, however, is only about 2 mbar between 25° and 75°, while the topographic effect is very much larger (about an 8 mbar range between Tharsis and Hellas), such that the areal effect on the TLWP is minimal. The activation of TLWP in the northern mid and high latitudes has already been mentioned for 45°. At 60° and 75° the area and duration of TLWP increase (Figures 6n, 6o, 6s, and 6t). The 25° and 35° obliquity cases are quite similar, with a slight decrease in the duration in TLWP being the most significant effect. This is again due to the strengthening CO₂ cycle and the decrease in the year-fraction with the subsolar point in the “tropics” (see section 4.1.2). During the first year of the lower obliquity (15°) simulation, only the rims of the Hellas and Argyre basins have TLWP (a thermal control effect), while the tropical TLWP distribution has greater longitudinal extent (due to the concentration of peak temperatures in the tropics). As the simulation continues, the surface pressure drops due to permanent cap formation, and TLWP regions disappear due to insufficient surface pressure.

4.2. Secular Change in Mean Surface Pressure

[29] The idea that the Martian atmosphere has decreased in thickness over geological history is supported directly by noble gas and isotopic data, and indirectly by morphological and geochemical evidence of stable, surficial liquid water in

the very distant past [Fanale *et al.*, 1992; Haberle, 1998; Jakosky and Phillips, 2001]. Increasing surface pressure is therefore representative of progressively earlier epochs in Martian climate history. In this section, we present simulations in which the climatically-available CO₂ is progressively doubled. These simulations are undertaken for current obliquity in section 4.2.1 and for high obliquity (45°) in section 4.2.2.

4.2.1. Contemporary Obliquity

[30] The variation of surface pressure for the standard obliquity pressure sequence is shown in Figure 7. The mean pressure approximately doubles between each simulation, reaching a global mean pressure of just over 1 bar in the p128x_std simulation. The global and annual mean surface pressures and the temperature increase relative to the 6 mbar case for these simulations are shown in Figure 2. Inspection of Figure 7 shows that for all simulations save for p1x_std (which is referred to previously as the o25 case), the pressures are everywhere well above 610 Pa. Thus the surface pressure constraint, which was so important for the simulations described in section 4.1, is no longer of concern.

[31] The trend in TLWP as a function of mean surface pressure is shown in Figures 8 and 9. As the surface pressure increases from the p1x_std to the p2x_std case, there is a very sharp increase in the total area of TLWP. As mentioned above, this increase is sufficient to remove the constraint on TLWP in the southern hemisphere, such that for p2x_std, there is TLWP at some point during the year for nearly the entire surface south of 30°N. This emphasizes the pressure-limited conditions presently (at a mean pressure of ~610 Pa) experienced over much of the planet, as only a small increase in atmospheric pressure opens up much of the surface to TLWP.

[32] As the mean pressure is increased above that of the p2x_std case, the area and duration of TLWP systematically decreases to a minimum in the p32x_std simulation (Figures 8 and 9). At this point, none of the GCM grid points report temperatures and pressures satisfying the TLWP criteria for any portion of any day. It is clear that pressure is not the limiting factor (Figure 7f). Instead, as shown in Figure 10f, the annually averaged maximum surface temperature has fallen to below 260 K. This decrease occurs despite the fact that the global-mean surface temperature is over 10 K warmer than the p1x_std contemporary simulation. Indeed, examination of Figure 10 shows that the average maximum daytime surface temperature decreases systematically between the p1x_std and the p32x_std cases. The increase in mean temperature and decrease in maximum temperature is obviously reconciled by the systematic decrease in the mean diurnal temperature range (Figures 11a–11f). From a peak of over 140 K in the p1x_std case, this range falls to a maximum of about 16 K in the p32x_std case, with 2 K being the typical range across much of the surface. The decrease in surface temperature range reflects the increased ability of the atmosphere to buffer surface temperatures. This is both a dynamical (the ability of the atmosphere to move heat to and from the surface, and from the dayside to nightside and equator to pole) and a thermal mass/radiative effect (an increase in the effective radiative timescale of the planet to well beyond one day), the latter probably being the greatest effect.

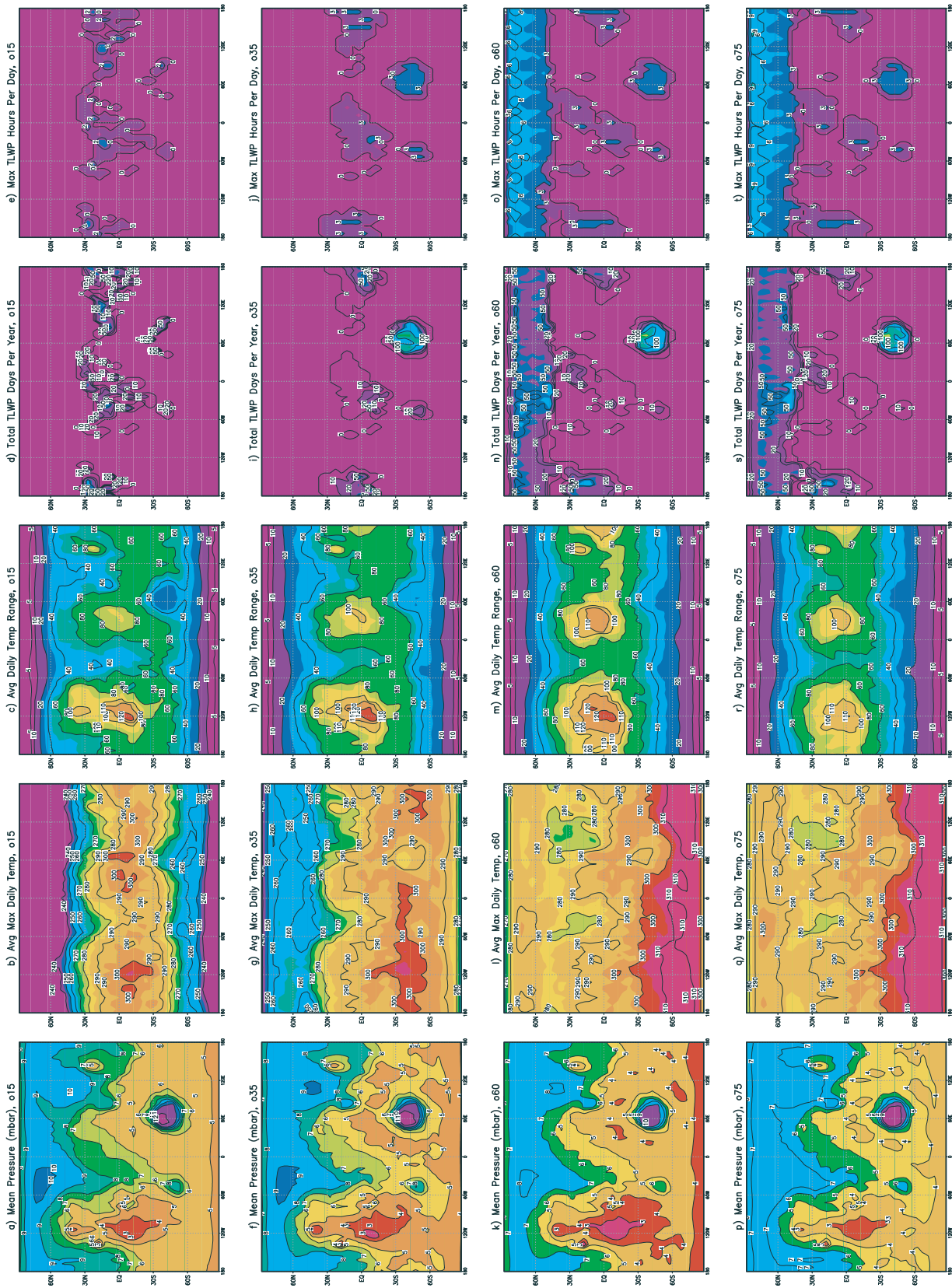


Figure 6. Same as Figure 4, but varying only obliquity (15°, 35°, 60°, and 75°). Eccentricity and argument of perihelion at current values.

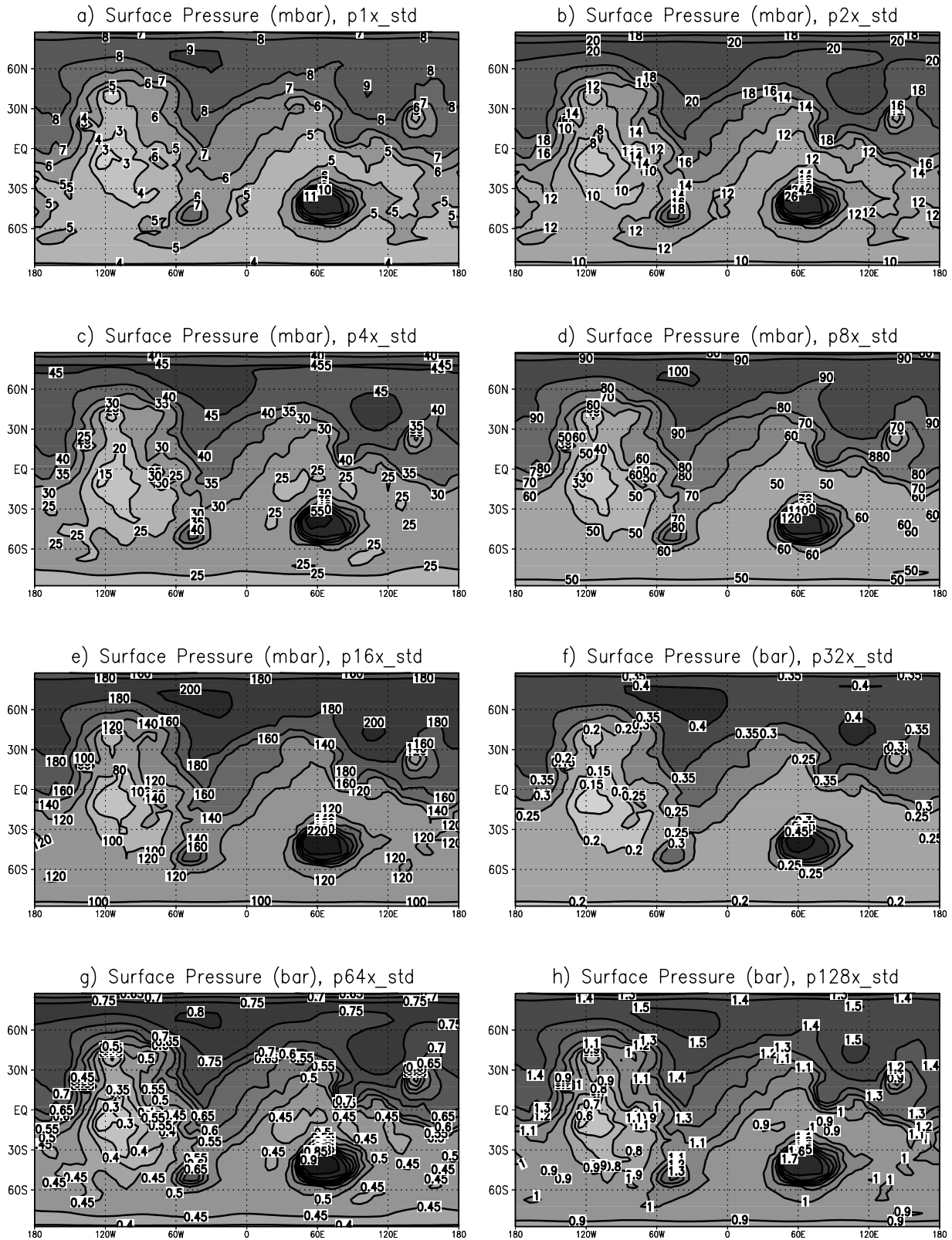


Figure 7. Variation of surface pressure for the p1x_std to p128x_std simulation sets.

[33] Increasing the mean pressure above that in the p32x_std case results in a slight increase in TLWP for the p64x_std case, which is related to the increase in mean surface temperature (Figure 2): the temperature

range is little changed from the p32x_std case (compare Figures 11f and 11g). By p128x_std, the mean surface pressure is sufficiently high that the overly-aggressive greenhouse effect in the GCM pushes mean surface

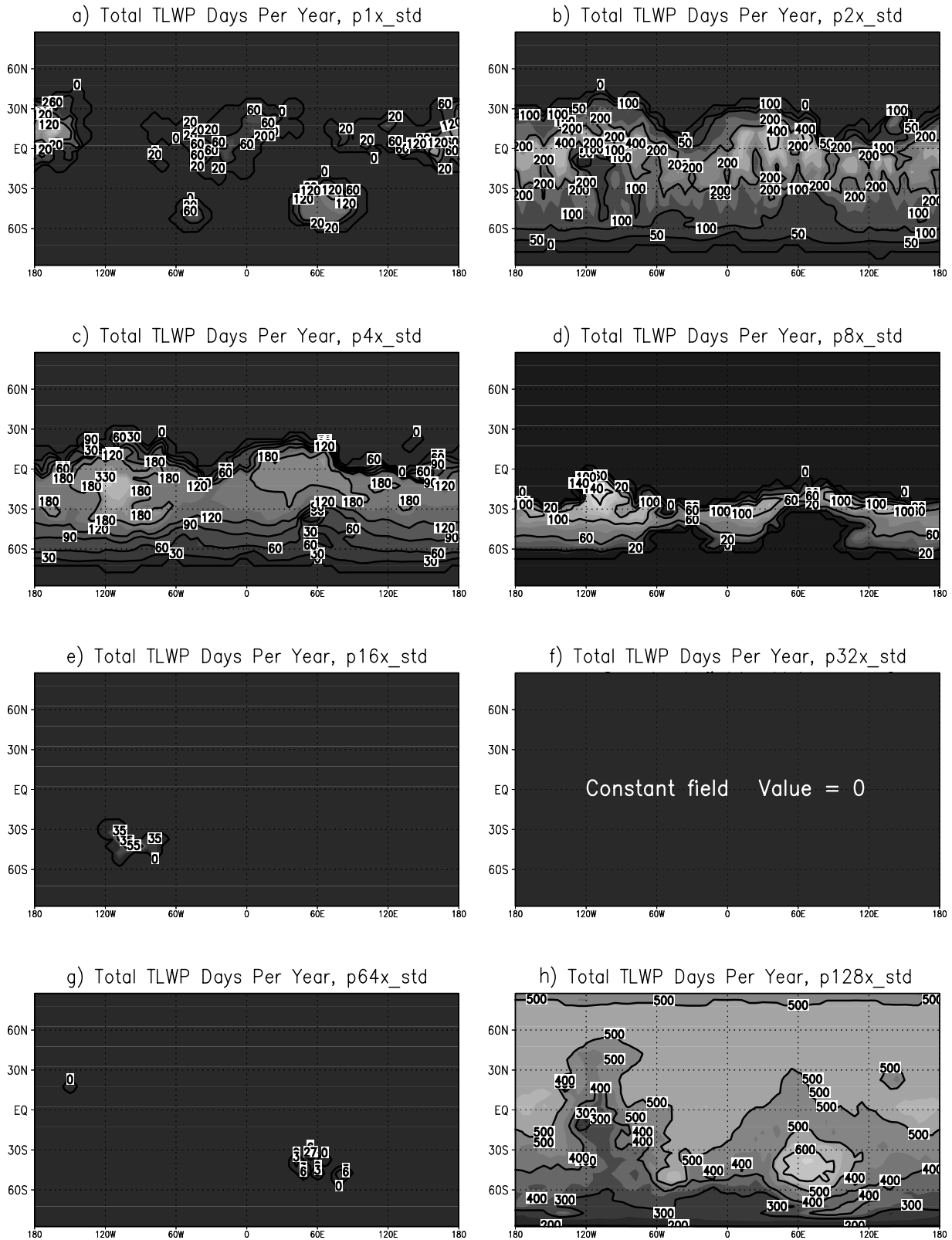


Figure 8. Days during which TLWP conditions were achieved for the p1x_std to p128x_std set.

temperatures above the melting point of ice (Figure 2 and Figure 10h). This results in widespread TLWP for long durations. However, this is a misnomer for the p128x_std, as this water is not transient; the surface

pressures and temperatures are consistent with truly stable liquid water.

[34] The GCM simulations of increasing mean surface pressure shows a distinctly nonmonotonic trend in TLWP.

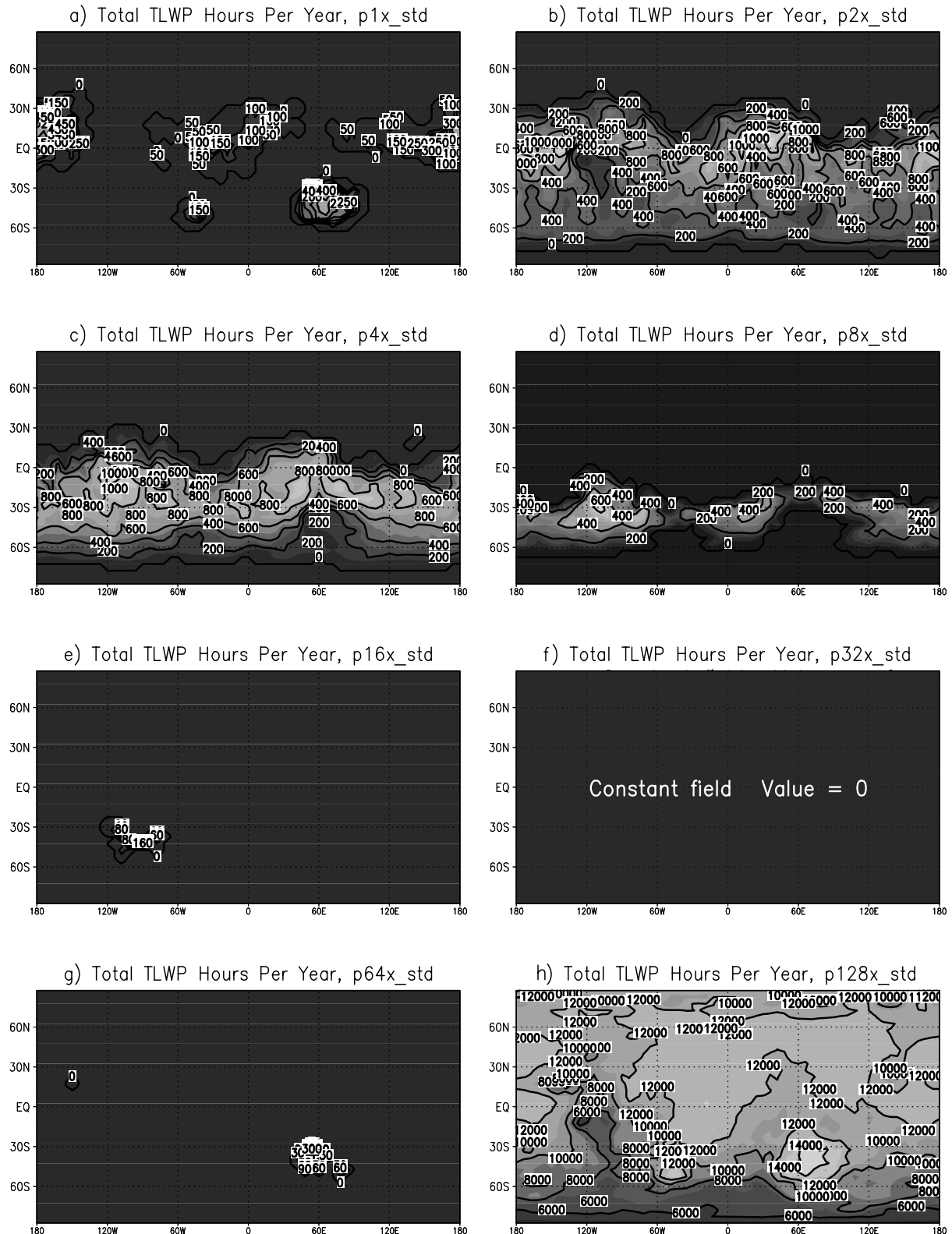


Figure 9. Same as Figure 7 but for cumulative hours of TLWP.

Indeed, these results suggest that Mars has likely passed through a “dead zone” of potential liquid water activity corresponding to the middle range of surface pressures between those of contemporary Mars and those required

to provide an “early, warm, wet” climate. The behavior of liquid water potential breaks into three distinct regimes: stable liquid water, thermally-controlled TLWP, and joint temperature- and pressure-controlled TLWP. The p128x_std

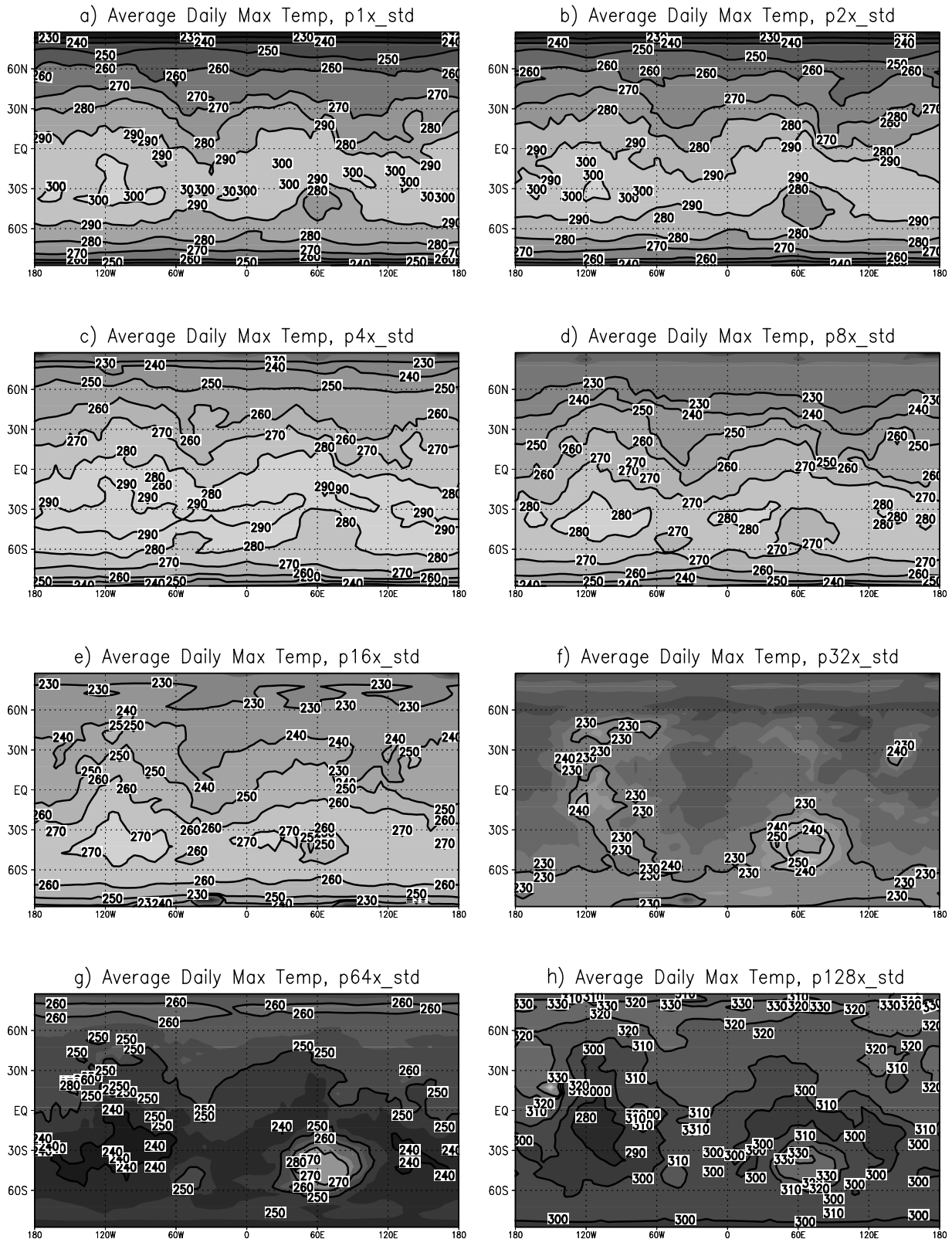


Figure 10. Same as Figure 7 but for annual-mean maximum daily surface temperature.

corresponds to the first regime, while the p1x_std is in the latter regime. For the rest of the simulations, the surface pressure everywhere is above the triple point pressure, such that only peak daytime temperatures provide a constraint on the geographical distribution of TLWP.

4.2.2. High Obliquity

[35] Simulations showing the effect of consecutive doubling of the available CO₂ inventory at the long-term mean obliquity of 45° are illustrated in Figure 12. The trend is the same as for the 25° obliquity simulations described in

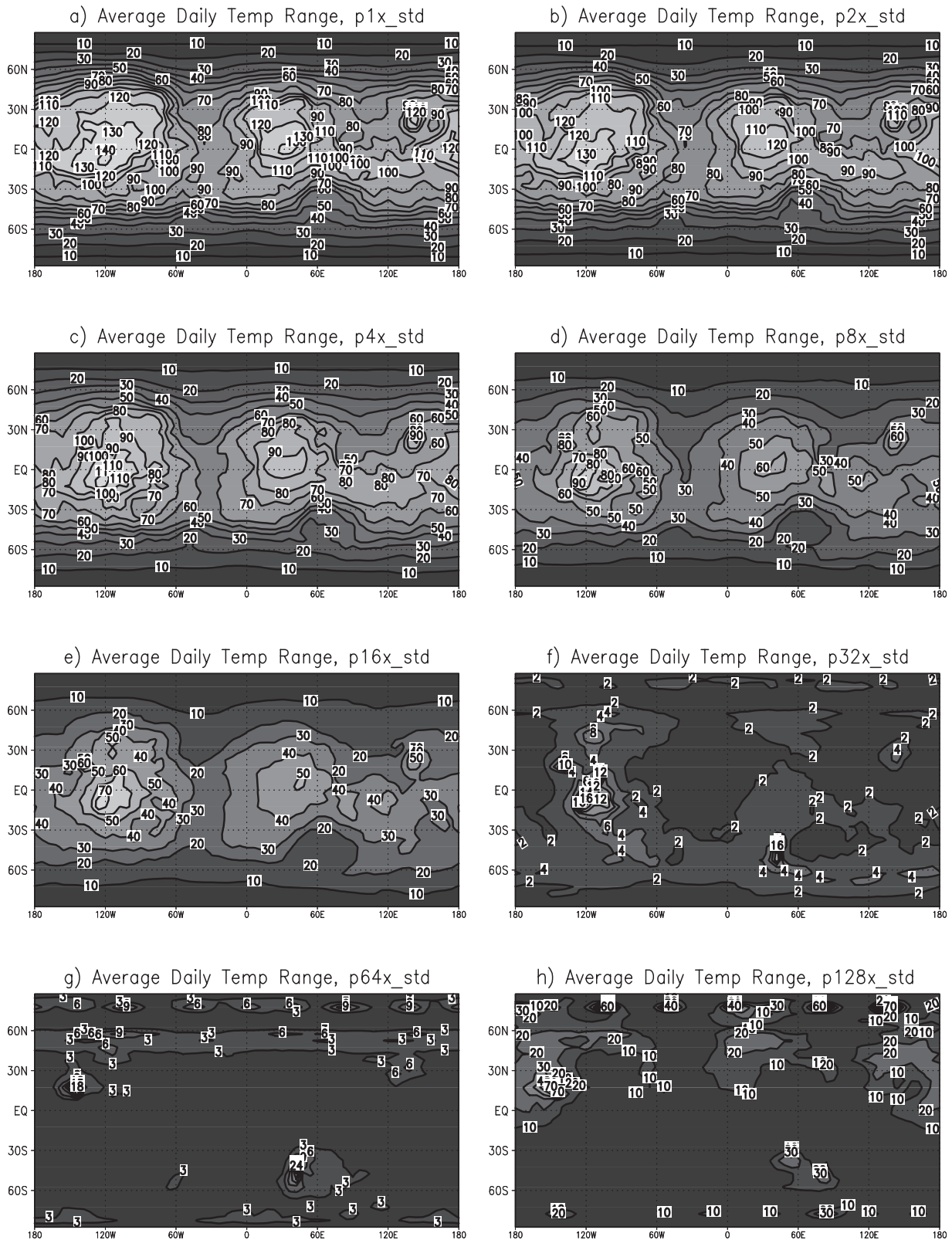


Figure 11. Same as Figure 7 but for the average daily temperature range.

section 4.2.1. The p128x_o45 case is not shown, but has stable liquid water like its counterpart. The p1x_o45 is a reproduction of the o45 case discussed in section 4.1. The northern band of TLWP is enabled by high surface pres-

ures, while the lack of TLWP in the south is a result of low surface pressure. For p4x_o45 (and p2x_o45, not shown), the southern hemisphere shows substantial TLWP (as for the 25° cases), but additionally has a band of TLWP in the

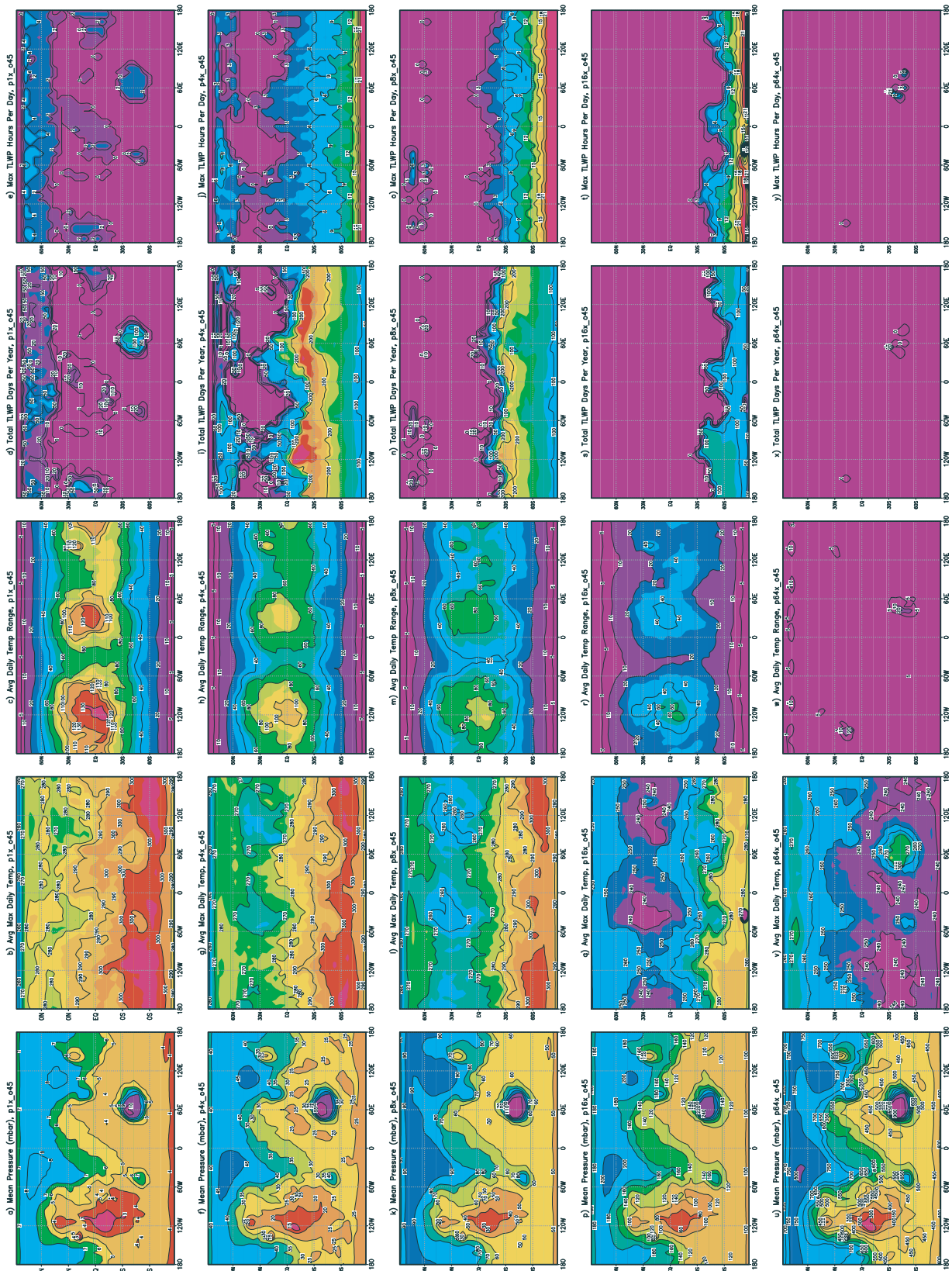


Figure 12. Same as Figure 4 but for the variation of mean surface pressure for an obliquity of 45° and contemporary eccentricity and argument of perihelion.

high northern latitudes associated with higher peak daytime temperatures during the northern summer, due to the more northward position of the subsolar latitude. As the mean pressure increases into the p16x_o45 to p64x_o45 cases, the daily temperature range again contracts faster than the mean temperature increases such that the peak daytime temperatures do not exceed the melting point. The increased obliquity does not allow the planet to escape the TLWP “dead zone” for the middle range of evolutionary mean surface pressures.

5. Discussion and Conclusions

[36] The argument we have put forth here suggests that there has not been a monotonic decrease in the ability to sustain liquid water on the surface over Martian history. Rather, following the earliest stages of Martian evolution, (possibly consisting of the “warm, wet” period) formation of liquid water on the surface for even short periods of time was much less likely over much of Martian history than it is on the planet today. Only relatively recently have conditions, namely daytime maximum temperatures, evolved back to the point at which liquid water is once again transiently plausible (Figure 13). The most likely epoch for formation of transient liquid water corresponds to surface pressures roughly double those of today, being sufficiently high to prevent boiling of any liquid water generated by ice-melt anywhere on the planet. Contemporary mean surface pressure is sufficiently low that vast areas of the southern hemisphere, where daytime temperatures frequently exceed the melting point, have no temperature separation between melting and boiling. A countervailing tendency is for increased pressures to yield greater buffering of daytime maximum temperatures that offsets the increase in mean surface temperatures until the pressures get considerably high (~ 1 bar). Thus maximum daytime temperatures correspond to the lowest possible pressures. We have termed the gap between the “early warm, wet” phase and the more recent maximum in transient liquid water potential the “dead zone” for dramatic effect and to underscore the nonmonotonic likelihood of liquid water. Throughout the study we have considered pure water. If brines are used, the areal extent and duration of TLWP increases. At intermediate pressures, however, the daily temperature range is sufficiently suppressed that maximum temperatures fall below the melting point of all but the very strongest plausible brines (see below). Thus, while the quantitative details of particular mapping of climatic states to particular durations and distributions of TLWP will vary with the purity of the water, the main finding of this study does not. It is also worth noting that the present GCM cannot resolve the true nuances of actual topography on scales of kilometers and smaller. One cannot assume that a result of zero TLWP in these simulations absolutely excludes the creation of small-scale deposits of liquid water under special circumstances. Small-scale variations in topography, for example, can establish isolated regions where the criteria for TLWP are met, though in surrounding areas, the TLWP is zero. (The canonical example of this is the potential formation of gullies on thermally-preferred slopes [Costard *et al.*, 2002].) In this light, our results provide a long-term guide to the relative ease of transient liquid water generation in a given

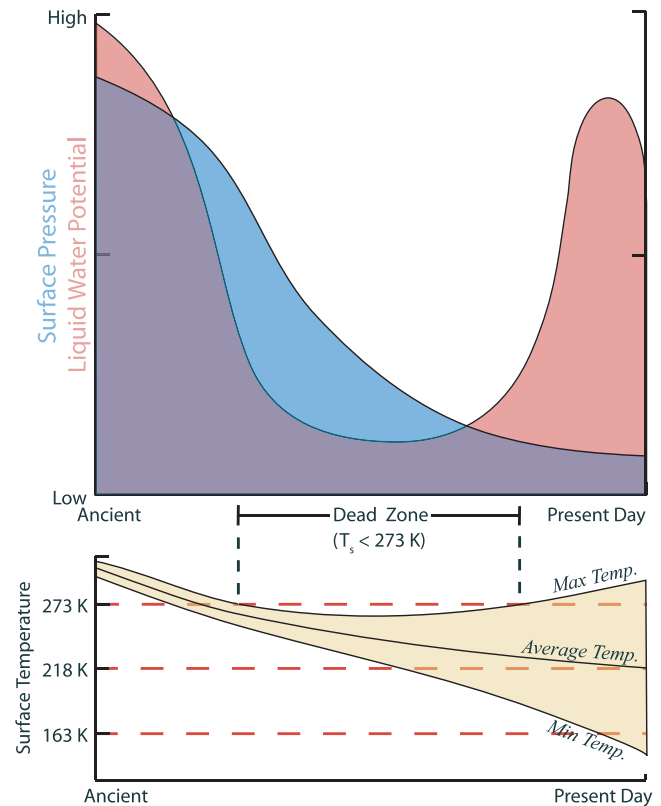


Figure 13. (a) Cartoon of the variation of TLWP and mean surface pressure over geological history. This variation results from (b) the competing effects of greenhouse warming of mean surface temperature and the impact of atmospheric buffering on the diurnal temperature range. At pressures near contemporary values, Figure 13a shows a decrease in TLWP as the surface pressure falls below the values needed to prevent boiling over much of the surface area of the planet.

area. Over time, the details of topography will have no effect on the long term evolution of TLWP discussed here. This evolution of TLWP suggested by this study has implications for how we interpret various morphological features on the Martian surface. This is particularly true for gullies and paleolakes, for which relatively recent ages have been suggested. The formation mechanism that produces gullies has been alternately suggested to be meltwater from surface ice [Costard *et al.*, 2002; Gilmore and Phillips, 2002; Hecht, 2002], bursting of shallow aquifers [Malin and Edgett, 2000; Mellon and Phillips, 2001], eruption of deep aquifers [Gaidos, 2001] or water melt at the base of dissipating snowpacks [Christensen, 2003], the first and last of which are greatly aided by (and may require) a shift to periods of high obliquity. We have not explored the formation of liquid water beneath the surface or below insulating layers of dust and/or surface ice here. For the gullies to be formed by surface meltwater also requires surface pressures to exceed the triple point. On the basis of superposition, Malin and Edgett [2000] argue that gullies are the youngest features in locations where they form, and are likely only a few million years in age. The observation of gullies in the southern hemisphere, which is presently

pressure-limited, calls upon one of two interpretations, either they were produced by surface melt but during a period when surface pressures were higher, or they were formed by one of the alternate scenarios, with no pressure limit.

[37] If we assume the gullies were formed by surface melt, then because of their very young age, secular CO₂ loss cannot account for a drop in pressure below the triple point in only 4 Myr (i.e., Mars likely has not lost the equivalent of 2–4 mbar in the past 4 Myr). We need, then, to consider other, periodic, oscillations in surface pressure. It has been suggested [Fanale and Salvail, 1994] that desorption of CO₂ in the regolith during high-obliquity conditions could result in higher surface pressures during these periods. As the southern hemisphere is presently only a few millibars below the triple point, it would not take much of an increase to permit liquid water. However, recent climate modeling [Armstrong et al., 2004] has indicated that at high obliquity, surface pressure may actually decrease, making it even harder to generate even transient liquid water. The response of atmospheric pressure to obliquity remains an unresolved question.

[38] Over the past 4 Myr, the Martian obliquity has risen to 35° [Touma and Wisdom, 1993; Laskar and Robutel, 1993] several times. Although the length of time at this extreme is $\sim 10^3$ years, this may be sufficient for numerous seasonal melt events to carve out the observed gullies. We may, then, be able to more accurately pinpoint the age of these gullies based upon the climate/obliquity results of Fanale and Salvail [1994] to the periods of maximum obliquity mentioned above. Alternatively, if the results from Armstrong et al. [2004] are truly representative of the pressure behavior at increasing obliquity, then this argues against surface melt as the origin of the gullies. Based upon the pressure restriction, it there would seem to be many more recent opportunities to generate meltwater in the northern hemisphere compared to the south, which is inconsistent with the observed gully distribution.

[39] Another type of surface feature for which this work has implications is the impact crater lake [Cabrol and Grin, 1999, 2001]. As discussed by H01, there is a strong correlation between the location of these paleolakes and the contemporary TLWP distribution. We suggest that this correlation is not coincidence, but rather the result of these specific regions permitting liquid water for extended periods over a wide range of orbital parameters.

[40] Relative to the age of these lakes (>0.5 Gyr), the orbital cycling period is quite short, meaning that such reservoirs will experience the full range of parameter space over their lifetime. As shown in Figures 4–6, the overall distribution of TLWP regions varies greatly with the specific orbital parameters, and, for conditions far from the present, there is a poor correlation between the observed location of these lakes and the regions with maximum TLWP. However, Figures 4–6 also reveal that in other orbital states, TLWP is not precluded from the present-day locations; they are simply not the dominant regions for most states. This provides an avenue by which these paleolakes can be sustained for extended periods of time. Mischna et al. [2003] have shown that surface ice is preferentially deposited in the tropical latitudes at high obliquity (>45°).

During those days where the TLWP criteria are met, small amounts of liquid water could form from the melting surface ice and be introduced to the ice-covered lake. The conditions required for this scenario have been modeled to be robust over a wide range of orbital states, yielding both the thermophysical and water requirements to produce the lakes.

[41] As stated previously, there are two requirements for liquid water to exist on the Martian surface, though to this point we have only addressed the thermophysical constraints, hence our choice of the term transient liquid water potential. The source of the water itself is uncertain, but must be restricted to one of two types of deposits, residual or seasonal. We have mentioned previously that regions of TLWP and residual surface ice are, logically, anticorrelated. Permanent deposits of ice cannot form in locations where temperatures regularly exceed the melting point. It is possible, however, for seasonal ice deposits to form in regions of TLWP during the winter, when liquid water is constrained by temperature. The exact mechanism by which seasonal ice can melt rather than boil is uncertain, though several hypotheses have been put forth [Hecht, 2002; Hecht and Bridges, 2003] to describe possible scenarios.

[42] Through this paper we have considered only pure water, with a melting point of 273 K, though several [Clark and Van Hart, 1981; H01; Knauth and Burt, 2002; Burt and Knauth, 2003] have considered the role of brines as a way to depress the melting point, and permit liquid on the Martian surface for temperatures as low as 220 K. Considering brine as the liquid opens up progressively more of the surface to TLWP for increasing salinity, not only the northern hemisphere (previously temperature limited), but the southern hemisphere as well. A depressed melting point lowers the saturation vapor pressure, serving to inhibit boiling, even under contemporary conditions.

[43] Of course, it is not guaranteed to achieve significant freezing point depressions. A melting temperature of 251 K corresponds to the NaCl eutectic, an optimal solution not necessarily ever achieved on the Martian surface. (It, in part, depends on the abundance of subsurface liquid water available to “dilute” the brine solution [Clifford, 1993]). While other chlorides (Fe³⁺ and Ca²⁺) have greater freezing point depressions, Clark and Van Hart [1981] conclude that the presence of soluble sulfates in the soil will react with the cations to form less effective “antifreeze” compounds. The conclusion of Clark and Van Hart [1981] is that NaCl is perhaps the most likely candidate to maximize freezing point depression. More recent studies by Knauth and Burt [2002] and Burt and Knauth [2003] argue that the presence of calcium chloride in dense brine solution is plausible under contemporary Martian conditions because of interactions between once-rich NaCl brine with calcium-rich basaltic regolith, allowing the formation of calcium chloride, and allowing eutectic temperatures as low as 220 K. Physically, a solution nearing its eutectic point will be relatively dense with a high viscosity and will behave more like molasses or softened glass than liquid water [Clark and Van Hart, 1981]. Assuming for the moment that large flows of a eutectic solution could form on the surface, its erosion properties would differ drastically from liquid water, and in

a manner that would appear inconsistent with the shape and morphology of the gullies, which, given their sharp features and alluvial fans, resemble terrestrial gullies formed by less viscous liquid (i.e., pure/near pure water) [Costard *et al.*, 2002].

[44] Thus the brine hypothesis shall remain just that, until future investigations are able to better determine the mineralogic composition of surface and subsurface salts. We therefore acknowledge that salty brines may permit the presence of “liquid” water on the surface for significantly depressed melting points. As noted by H01, this opens up the entire surface to TLWP at some point during the year. This also removes the pressure limitation in the southern hemisphere, as noted by H01, an NaCl eutectic solution at 251 K will have a vapor pressure below the atmospheric value everywhere on the planet. We do note, however, that as these brines approach their eutectic point, they become thicker and more viscous, and it becomes more difficult to explain the gully formation. Certainly the visible appearance of the gullies suggests rapid fluvial flow rather than the slow, halting movement of a viscous solution.

[45] This problem is far from resolved. Future work in this area will be geared toward a more precise representation of the various radiative processes that will affect these results. One significant process yet to be considered is the amount of greenhouse warming provided by increasing levels of water vapor in thicker Martian atmospheres. Presently, there is minimal warming by water vapor, however, for significantly thicker atmospheres (hundreds of mbar to several bars), the more humid atmosphere may generate many tens of degrees of greenhouse warming. The effects of clouds, of both liquid and CO₂ composition, must also be considered in future work to yield a higher-fidelity mapping between the modeled mean surface pressure and the particular surface greenhouse warming. Finally, coupling the model with a full water cycle for the higher-pressure states would provide a third constraint on TLWP: water ice availability for melting.

[46] **Acknowledgments.** This work was supported by the NASA Mars Fundamental Research Program. Thanks to Steve Clifford and an anonymous reviewer.

References

- Armstrong, J. C., C. B. Leovy, and T. Quinn (2004), A 1 Gyr climate model for Mars: New orbital statistics and the importance of seasonally resolved polar processes, *Icarus*, *171*, 255–271.
- Boynton, W. V., et al. (2002), Distribution of hydrogen in the near surface of Mars: Evidence for subsurface ice deposits, *Science*, *297*, 81–85.
- Briegleb, B. P. (1992), Delta-Eddington approximation for solar radiation in the NCAR community climate model, *J. Geophys. Res.*, *97*, 7603–7612.
- Burk, S. D. (1976), Diurnal winds near the Martian polar caps, *J. Atmos. Sci.*, *33*, 923–949.
- Burt, D. M., and L. P. Knauth (2003), Electrically conducting, Ca-rich brines, rather than water, expected in the Martian subsurface, *J. Geophys. Res.*, *108*(E4), 8026, doi:10.1029/2002JE001862.
- Cabrol, N. A., and E. A. Grin (1999), Distribution, classification, and ages of Martian impact crater lakes, *Icarus*, *142*, 160–172.
- Cabrol, N. A., and E. A. Grin (2001), The evolution of lacustrine environments on Mars: Is Mars only hydrologically dormant?, *Icarus*, *149*, 291–328.
- Carr, M. H. (1996), *Water on Mars*, 229 pp., Oxford Univ. Press, New York.
- Christensen, P. R. (1986), Regional dust deposits on Mars: Physical properties, age and history, *J. Geophys. Res.*, *91*, 3533–3545.
- Christensen, P. R. (2003), Formation of recent Martian gullies through melting of extensive water-rich snow deposits, *Nature*, *422*, 45–48.
- Clark, B. C., and D. C. Van Hart (1981), The salts of Mars, *Icarus*, *45*, 370–378.
- Clifford, S. M. (1993), A model for the hydrologic and climatic behavior of water on Mars, *J. Geophys. Res.*, *98*, 10,973–11,016.
- Costard, F., F. Forget, N. Mangold, and J. P. Peulvast (2002), Formation of recent Martian debris flows by melting of near-surface ground ice at high obliquity, *Science*, *295*, 110–113.
- Fanale, F. P., and J. R. Salvail (1994), Quasi-periodic atmosphere-regolith-cap CO₂ redistribution in the Martian past, *Icarus*, *111*, 305–316.
- Fanale, F. P., S. E. Postawko, J. B. Pollack, M. H. Carr, and R. O. Pepin (1992), Mars: Epochal climate change and volatile history, in *Mars*, edited by H. H. Kieffer et al., pp. 1135–1179, Univ. of Ariz. Press, Tucson.
- Feldman, W. C., et al. (2002), Global distribution of neutrons from Mars: Results from Mars Odyssey, *Science*, *297*, 75–78.
- Fenton, L. K., and M. I. Richardson (2001), Martian surface winds: Insensitivity to orbital changes and implications for aeolian processes, *J. Geophys. Res.*, *106*, 32,885–32,902.
- Gaidos, E. J. (2001), Cryovolcanism and the recent flow of liquid water on Mars, *Icarus*, *153*, 218–223.
- Gilmore, M. S., and E. L. Phillips (2002), Martian aquicludes required for gully formation, *Eos Trans. AGU*, *83*(47), Fall Meet. Suppl., Abstract P72C-09.
- Gough, D. O. (1981), Solar interior structure and luminosity variations, *Sol. Phys.*, *74*, 21–34.
- Haberle, R. M. (1998), Early Mars climate models, *J. Geophys. Res.*, *103*, 28,467–28,479.
- Haberle, R. M., C. B. Leovy, and J. B. Pollack (1982), Some effects of global dust storms on the atmospheric circulation of Mars, *Icarus*, *50*, 322–367.
- Haberle, R. M., C. P. McKay, J. Schaeffer, N. A. Cabrol, E. A. Grin, A. P. Zent, and R. Quinn (2001), On the possibility of liquid water on present-day Mars, *J. Geophys. Res.*, *106*(E10), 23,317–23,326.
- Hecht, M. H. (2002), Metastability of liquid water on Mars, *Icarus*, *156*, 373–386.
- Hecht, M. H., and N. T. Bridges (2003), A mechanism for recent production of liquid water on Mars, *Lunar Planet. Sci.*, *XXXIV*, Abstract 2073.
- Hinson, D. P., and R. J. Wilson (2002), Transient eddies in the southern hemisphere of Mars, *Geophys. Res. Lett.*, *29*(7), 1154, doi:10.1029/2001GL014103.
- Hinson, D. P., and R. J. Wilson (2004), Temperature inversions, thermal tides, and water ice clouds in the Martian tropics, *J. Geophys. Res.*, *109*, E01002, doi:10.1029/2003JE002129.
- Hourdin, F. (1992), A new representation of the absorption by the CO₂ 15-micron band for a Martian general circulation model, *J. Geophys. Res.*, *97*, 18,319–18,335.
- Ingersoll, A. P. (1970), Mars: Occurrence of liquid water, *Science*, *168*, 972–973.
- Jakosky, B. M. (1985), The seasonal cycle of water on Mars, *Space Sci. Rev.*, *41*, 131–200.
- Jakosky, B. M., and C. B. Farmer (1982), The seasonal and global behavior of water vapor in the Mars atmosphere: Complete global results of the Viking atmospheric water detector experiment, *J. Geophys. Res.*, *87*, 2999–3019.
- Jakosky, B. M., and R. J. Phillips (2001), Mars’ volatile and climate history, *Nature*, *412*, 237–244.
- Kahn, R. (1985), The evolution of CO₂ on Mars, *Icarus*, *62*, 175–190.
- Kasting, J. F. (1991), CO₂ condensation and the climate of early Mars, *Icarus*, *94*, 1–13.
- Knauth, L. P., and D. M. Burt (2002), Eutectic brines on Mars: Origin and possible relation to young seepage features, *Icarus*, *158*, 267–271.
- Laskar, J., and P. Robutel (1993), The chaotic obliquity of the planets, *Nature*, *361*, 608–612.
- Laskar, J., A. C. M. Correia, M. Gastineau, F. Joutel, B. Levrard, and P. Robutel (2004), Long term evolution and chaotic diffusion of the insolation quantities of Mars, *Icarus*, *170*, 343–364.
- Malin, M. C., and K. S. Edgett (2000), Evidence for recent ground water seepage and surface runoff on Mars, *Science*, *288*, 2330–2335.
- Mellon, M. T., and R. J. Phillips (2001), Recent gullies on Mars and the source of liquid water, *J. Geophys. Res.*, *106*(E10), 23,165–23,180.
- Mischna, M. A., M. I. Richardson, R. J. Wilson, and D. J. McCleese (2003), On the orbital forcing of Martian water and CO₂ cycles: A general circulation model study with simplified volatile schemes, *J. Geophys. Res.*, *108*(E6), 5062, doi:10.1029/2003JE002051.
- Mitrofanov, I., et al. (2002), Maps of subsurface hydrogen from the High Energy Neutron Detector, Mars Odyssey, *Science*, *297*, 78–81.

- Richardson, M. I., and R. J. Wilson (2002), Investigation of the nature and stability of the Martian seasonal water cycle with a general circulation model, *J. Geophys. Res.*, *107*(E5), 5031, doi:10.1029/2001JE001536.
- Svitek, T., and B. Murray (1990), Winter frost at Viking Lander 2 site, *J. Geophys. Res.*, *95*, 1495–1510.
- Touma, J., and J. Wisdom (1993), The chaotic obliquity of Mars, *Science*, *259*, 1294–1296.
- Wilson, R. J. (1997), A general circulation model simulation of the Martian polar warming, *Geophys. Res. Lett.*, *24*, 123–127.
- Wilson, R. J., and K. P. Hamilton (1996), Comprehensive model simulation of thermal tides in the Martian atmosphere, *J. Atmos. Sci.*, *53*, 1290–1326.
- Wilson, R. J., and M. I. Richardson (2000), The Martian atmosphere during the Viking mission, I. Infrared measurements of atmospheric temperatures revisited, *Icarus*, *145*, 555–579.
- Wilson, R. J., D. Banfield, B. J. Conrath, and M. D. Smith (2002), Traveling waves in the northern hemisphere of Mars, *Geophys. Res. Lett.*, *29*(14), 1684, doi:10.1029/2002GL014866.
-
- M. A. Mischna, Jet Propulsion Laboratory, California Institute of Technology, Pasadena, CA 91109, USA.
- M. I. Richardson, Division of Geological and Planetary Sciences, California Institute of Technology, MS 150-21, Pasadena, CA 91125, USA. (mir@gps.caltech.edu)